Research Article | Vol. 27, No. 24 / 25 November 2019 / Optics Express 35865
Optics EXPRESS

Pump-induced lensing effects in diode pumped Alexandrite lasers

GORONWY TAWY,* JIAN WANG, AND MICHAEL J. DAMZEN

Photonics Group, The Blackett Laboratory, Dept. of Physics, Imperial College London, Prince Consort Road, London SW7 2AZ, UK
goronwy.tawy12@imperial.ac.uk

Abstract: It is essential to understand the pump-induced lensing and aberration effects in solid-state lasers, such as Alexandrite, since these set limits on laser power scaling whilst maintaining high spatial TEM_{00} beam quality. In this work, we present direct wavefront measurements of pump-induced lensing and spherical aberration using a Shack-Hartmann wavefront sensor, for the first time, in a diode-pumped Alexandrite laser, and under both non-lasing and lasing conditions. The lens dioptric power is found to be weakly sub-linear with respect to the absorbed pump power, and under lasing, the lensing power is observed to decrease to 60 % of its non-lasing value. The results are inconsistent with a thermal lens model but a fuller theoretical formulation is made of a combined thermal and population lens model giving good quantitative agreement to the observed pump power dependence of the induced-lensing under non-lasing conditions and the reduced lensing under lasing conditions. The deduced value for the difference in excited to ground state polarizability is consistent with prior measurement estimates for other chromium-doped gain media. The finding of this paper provide new insight into pump-induced lensing in Alexandrite and also provides a basis for a fast saturable population lens mechanism to account for self-Q-switching observed recently in Alexandrite laser systems.

1. Introduction

Pump-induced lensing and refractive index aberration effects in the laser gain medium are primary problems that limit power scaling and maintenance of high spatial quality in many lasers, and especially in solid-state lasers. Understanding and measuring pump-induced lensing effects in solid-state lasers, particularly in diode-end-pumped laser configurations, are useful and often essential for providing suitable resonator designs for high spatial TEM_{00} beam quality with good efficiency when attempting to operate at increased powers [1,2].

A primary lensing mechanism is the heat deposition in the gain medium. Theoretical modelling of the heat diffusion equation has provided analytical solutions for the lensing power under a number of simplifying assumptions [1–8]. More complete theoretical solutions can be found by using numerical simulations with full 3-D finite element analysis (FEA) methods that do not need to be limited by simplifying assumptions. Various experimental methods for thermal lens measurement have been devised based on different principles and implementations [9]. These methods include: simply passing a probe beam through the laser medium and finding its focus distance to deduce the thermally induced lens dioptric power [10]; laser cavity stability and mode size measurements utilising standard laser cavity ABCD analysis [4]; wavefront measurements from classical fringe analysis; lateral shearing interferometry [11] and use of Shack-Hartmann wavefront sensors [12].

Alexandrite (Cr-doped chrysoberyl) is a vibronic solid-state laser material with broadly tunable lasing capability (701-858 nm) and excellent thermo-mechanical properties that make it suitable for high power operation [13,14]. Its broad absorption spectrum in the visible region means it

#377778 https://doi.org/10.1364/OE.27.035865
Journal © 2019 Received 18 Sep 2019; revised 6 Nov 2019; accepted 11 Nov 2019; published 21 Nov 2019

Optics EXPRESS

can be directly diode-pumped using red (AlGaInP) laser diodes, offering the potential for high efficiency. Demonstrations of diode-pumping of Alexandrite have been made in end-pumped rod [15–18] and side-pumped slab [19]. Laser power up to 26.2 W [16], slope efficiency up to 54 % [17] and wavelength tuning range >100nm [15,17] shows the potential for significant power scaling, good efficiency and broad tunability of diode-pumped Alexandrite.

Alexandrite has a long upper-state lifetime of 262 µs at room temperature [13], making it favourable for high energy Q-switched operation under diode-pumping. Demonstrations have been made of active [20], single-longitudinal-mode [21], and passively [22] Q-switched Alexandrite lasers. The broad emission band of Alexandrite also has potential for modelocked ultra-short pulse formation, down to ~ 10fs, in principle. Recently, demonstrations have been made of Kerr lens modelocking [23] as well as passive saturable absorber modelocking down to 65 fs [24].

For the high-power development of the Alexandrite laser and further enhancement of its performance for future potential tunable laser applications including lidar, spectroscopy, bio-photonics and quantum technologies it is important to have a good fundamental understanding of underlying mechanisms and material parameters relevant to the pump-induced lensing and aberration effects. However, to date, only one study has been conducted on the pump-induced lensing in a green-laser-pumped Alexandrite laser [25]. This study was based on an indirect ABCD propagation mode analysis with approximations and simplifying assumptions of the lensing results that limit the fundamental understanding of the underlying physical lensing mechanisms and also the extrapolation of the results to the prediction of lensing under other experimental pumping conditions.

The purpose of this paper is to provide an in-depth systematic investigation of pump-induced lensing effects in diode-pumped Alexandrite. For the first time, we perform a direct wavefront measurement of the diode-end-pumped Alexandrite crystal using a Shack-Hartmann wavefront sensor (SH-WFS). This provides a very accurate and direct full 2-D mapping of the pump-induced refractive index change to measure the net lensing power, without need for indirect interpretation, as well as providing information on the lensing aberrations with excellent measurement sensitivity (typically ~1/100th wavelength, for SH-WFS). In this paper, the lensing measurements as function of absorbed pump power are also performed under both non-lasing and laser conditions, again for the first time in Alexandrite. The lasing lens dioptric power shows a significant decrease to 60 % of the non-lasing case. A detailed theoretical analytical modelling of the thermally-induced lensing is conducted for Alexandrite due to quantum defect heating and incorporating the additional heating impact of pump excited-state absorption that is known to exist in Alexandrite [26]. Numerical modelling is also performed using finite element analysis (FEA) to incorporate more realistically the spatial pump distribution in the laser crystal. A notable discrepancy is found between the experimental non-lasing lens dioptric power that is observed to have a weakly sub-linear dependence with absorbed pump power whilst the theoretical thermal lens model with a nonlinear excited state absorption heating factor should lead to a super-linear dependence. The physical origin of the observed significant decreased lens dioptric power under lasing conditions then also becomes unclear. We find that introduction of a more complex analytical modelling based on a combined thermal lens and a population lens arising from difference in polarizability of excited and ground state ion populations gives not only a qualitative explanation of the observed experimental pump-induced lensing results but also good quantitative agreement of the pump power dependence under both non-lasing and lasing regimes. The pump dependent strength of spherical thermal aberration is also quantified experimentally under both lasing and non-lasing conditions in Alexandrite. The paper concludes with summary of some key new insights gained and numerical values for pump-induced lensing in Alexandrite. The population lensing provides a mechanism for self-Q-switching recently observed in Alexandrite [27] and suggestions are made for future studies for further verification and insight.

Optics EXPRESS

2. Pump induced lensing

2.1. Thermal lensing

Under optical pumping heat is deposited in the gain medium causing temperature increase and redistribution by internal heat transport that induces changes to the medium refractive index due to its temperature dependence. Additional refractive index changes occur due to thermal expansion causing surface deformation and stress-induced photo-elastic refractive changes and birefringence [1,2,7]. For the cases to be considered in this paper with continuous-wave optical pumping, the temperature distribution $T(r,z)$ can be described by the steady-state heat diffusion equation [7] and for axi-symmetric end-pumping of a laser rod in cylindrical coordinates (r,ϕ,z) is given by

$$\frac{1}{r}\frac{\partial}{\partial r}\left(r\frac{\partial T}{\partial r}\right)+\frac{\partial^2 T}{\partial z^2}=-\frac{Q(r,z)}{K_c} \tag{1}$$

where K_c is the thermal conductivity of the gain medium and $Q(r,z)=\alpha_0\eta_h I(r,z)$ is the heat power per unit volume generated by absorption of pump intensity $I(r,z)$, α_0 is the pump absorption coefficient and η_h is the fraction of absorbed pump radiation converted to heat.

Equation (1) can be solved for the temperature distribution by neglecting axial heat flow and assuming a non-diffracting, exponentially-absorbed pump intensity $I(r,z)=I(r,0)\exp(-\alpha_0 z)$. Two special pump distributions of interest are the 'top-hat' beam and Gaussian beam. For the 'top-hat' pump beam with incident pump power P_0 and radius w_p, with uniform intensity $I(r,0)=P_0/\pi w_p^2$ for $r\le w_p$ and $I(r,0)=0$ for $r>w_p$, solution of Eq. (1) gives a temperature profile that is quadratic in radial coordinate r for $r\le w_p$. This results in a quadratic transverse path length variation over rod length l producing an aberration-free lens within the $r\le w_p$ region with dioptric power (inverse of focal length f_T) given by

$$D_T=\frac{1}{f_T}=\frac{P_{abs}\chi\eta_h}{2\pi w_p^2 K_c} \tag{2}$$

where $P_{abs}=P_0[1-\exp(-\alpha_0 l)]$ is the absorbed pump power and χ is an effective thermo-optic coefficient. In the simplest analysis, often assumed in calculations for thermal lensing, χ is the temperature coefficient of refractive index $\chi_n=dn/dT$. In reality, due to thermal expansion there is an overall "effective" thermo-optic coefficient $\chi=\chi_n+\chi_{SB}+\chi_{PE}$ comprising three lensing contributions: the first is due to temperature-dependent refractive index ($\chi_n=dn/dT$); the second is a surface end bulging term, χ_{SB}; and the third is a stress-induced photoelastic refractive index lensing term, χ_{PE}. For an infinitely thin crystal $\chi_{SB}=(n-1)(1+\nu)\alpha_T$ where n is the unperturbed refractive index, ν is the Poisson's ratio, and α_T is the thermal expansion coefficient [7]. This "thin-crystal" approximation for the surface bulging should be treated very much as an upper limit and its contribution in a real crystal can be much less [7]. The photoelastic term ($\chi_{PE}=2n_0^3\alpha_T C'_{r,\theta}$) is a stress-induced refractive index contribution with cylindrical-symmetry induced birefringent principle axes [1,7]. This birefringence can cause depolarisation degradation of laser light, especially in isotropic crystals (e.g. YAG) but is much less problematic in laser crystals with strong natural birefringence (e.g. Alexandrite).

For the Gaussian pump beam with incident pump intensity $I(r,0)=(2P_0/\pi w_p^2)\exp(-2r^2/w_p^2)$, the temperature distribution is no longer a simple quadratic function and one can consider a thermal lens whose dioptric power varies radially, given by

$$D_T(r)=\frac{1}{f_T(r)}=\frac{P_{abs}\chi\eta_h}{\pi w_p^2 K_c}\frac{\left[1-\exp\left(-2r^2/w_p^2\right)\right]}{2r^2/w_p^2}. \tag{3}$$

The Gaussian pump beam induces a maximum lensing dioptric power on axis $D_T(0)$ twice as strong as the top-hat case. The radially-varying lensing becomes more aberrating as the transverse

Optics EXPRESS

size of an interacting laser beam increases and can lead to spatial mode degradation in a laser system.

2.2. Influence of heating mechanisms to thermally-induced lensing in laser crystal

The fractional heating factor η_h is a very important term to consider for thermally-induced lensing. In an "ideal" four-level optically-pumped laser material, each absorbed pump photon at wavelength λ_p results in an emitted optical photon with wavelength λ_o and the heating factor $\eta_h = \eta_d = 1 - \eta_s$ equals the quantum defect η_d and where $\eta_s = \lambda_o/\lambda_p$ is the Stokes efficiency, the ratio of the emitted optical to pump photon energies. Under strong lasing, stimulated emission dominates and $\lambda_o = \lambda_l$ is the lasing wavelength; under non-lasing conditions the spontaneous emission photon $\lambda_o = \lambda_f$ is the average fluorescence wavelength, which can be significantly different to the laser wavelength in a broad emission gain medium, such as Alexandrite. Most real solid-state materials deviate significantly from a simple four-level system and other sources of heating are present including non-radiative losses [28], excited state absorption (ESA) [26] and energy transfer upconversion (ETU) [29] that can contribute to a significantly higher heating factor than the quantum defect. The strength of ESA and ETU heating mechanisms are dependent on the excited state population density. This leads to the heating factor η_h having a nonlinear intensity dependence and its value will vary spatially according to the local intensity, contributing to further aberration effects.

Figure 1 shows the simplified energy level diagram for Alexandrite. Laser emission occurs at the ${}^4T_2 \rightarrow {}^4A_2$ transition. The broadband excited vibronic state ${}^4T_2$ is in thermal equilibrium with closely situated ($\Delta E = 800$ cm^{-1}) long-lived storage state ${}^2E$ such that it can be modelled as a combined upper-laser level with total population n_1 with a temperature dependant effective stimulated emission cross section and fluorescence lifetime [26]. The figure also indicates pump and laser ground-state absorption (GSA) and pump and laser excited state absorption (ESA) to higher energy levels. Notation used in this paper for their various associated absorption/emission cross-sections and non-radiative transitions are also indicated. No ETU has been identified in Alexandrite but ESA is a known mechanism that occurs at the pump and lasing wavelengths [13,26]. The contribution of pump ESA to the overall heating can be included to obtain a more general form for the heating factor via a modified pump quantum efficiency term η_p [26]

$$\eta_h = 1 - \eta_s \eta_p. \tag{4}$$

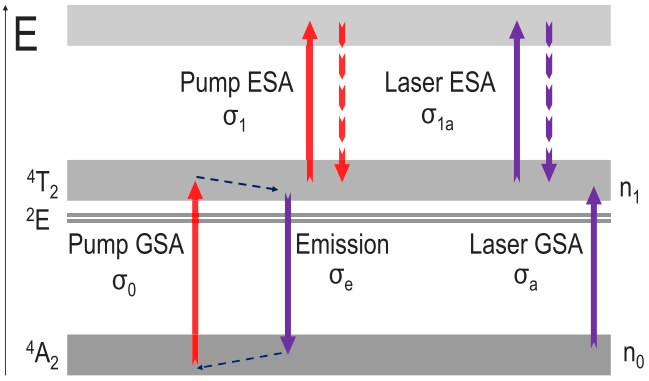

Fig. 1. Energy levels of Alexandrite showing electronic transitions and their respective cross sections with broad bands representing the vibrational levels. Non-radiative transitions are shown as dashed lines.

Optics EXPRESS

The pump quantum efficiency η_p is the probability that an absorbed pump photon generates an upper-laser level population. The intrinsic pump quantum efficiency (or quantum yield) η_{p0} is the branching probability of a pump-excited ion reaching the upper-state laser level (leading to radiative spontaneous or stimulated emission) compared to other pathways for the excited ion to return to the ground state non-radiatively. In the non-radiative case, all the pump photon energy will be dissipated in the gain medium as heat. In Alexandrite, the quantum yield factor η_{p0} is usually taken as unity [13]. The presence of ESA and ETU processes can also be incorporated into the heating factor by considering them as additional terms that decrease the pump quantum efficiency [30]. In the case of pump ESA, pump photons are absorbed via ions in the upper laser level without contributing to an increase in inversion population and is a direct contribution to reduction of the effective pump quantum efficiency. In the case of ETU, upper-state population previously generated by pump photons is subsequently lost without radiative emission, and can be considered a step-wise reduction in pump quantum efficiency. Since ETU is not present in Alexandrite our attention in this paper will be to consider just the contribution due to pump ESA.

The full analytical modelling of pump ESA and its impact on pump quantum efficiency, and hence heating, has been recently developed [26,30]. The pump quantum efficiency $\eta_p = \eta_{p0}\eta_{p,esa}$ is a product of the intrinsic quantum efficiency η_{p0} and a pump ESA efficiency $\eta_{p,esa}$ [30]. The pump ESA efficiency $\eta_{p,esa}$ is the ratio of the (useful) pump ground state absorption (GSA) that leads to inversion generation to the total pump ground-state absorption (GSA) plus excited state absorption (ESA). With rate of pump GSA $\sigma_0 n_0$, rate of pump ESA $\sigma_1 n_1$ and total active laser ion population $N = n_0 + n_1$ (sum of the ground-state population n_0 and upper-laser population n_1), we can define a "local" pump ESA efficiency

$$\eta_{p,esa} = \frac{\sigma_0 n_0}{\sigma_0 n_0 + \sigma_1 n_1} = \frac{1-f}{1+(\gamma-1)f} \tag{5}$$

where $f = n_1/N$ is the fractional inversion and $\gamma = \sigma_1/\sigma_0$ is the ratio of the pump ESA cross-section to pump GSA cross-section. When $\gamma = 0$, $\eta_{p,esa} = 1$, but when $\gamma \neq 0$, $\eta_{p,esa}$ will decrease from unity with increasing fractional inversion f. The pump power absorbed from pump ESA is directly transferred to heat. It is assumed in the modelling that the pump ESA that takes the excited state ion to a higher-lying level is rapidly (but non-radiatively) returned back to the excited upper-laser level. As such, pump ESA does not deplete the inversion but any pump ESA photons lost make no net contribution to increasing the population inversion.

The full mathematical formulation to derive the pump ESA quantum efficiency requires solution of the coupled pump absorption and material rate equations and will be detailed in Section 5 of this paper. It suffices to note here that since the strength of pump ESA increases with excited state population density then the pump ESA efficiency $\eta_{p,esa}$ will decrease with higher pumping power, and the corresponding heating factor η_h will increase, according to Eq. (4). In its lowest-order form $\eta_h = \eta_{h0} + a_0 P_{abs}$ and hence the nonlinear form of the dioptric lens power $D_T = a_1 P_{abs} + a_2 P_{abs}^2$, where a_i are the coefficients, will lead to a graph of the lens dioptric power that is super-linear (due to term $a_2 P_{abs}^2$) with respect to absorbed pump power. We will return to this after the experimental results in Section 4 of this paper.

2.3. Population lensing

Refractive index changes can also be induced by changes to the excited state population density due to the difference in the polarizability of excited and ground state ions. The spatial variation of the excited population and therefore refractive index difference induces an electronic, or population lens. The effect has been observed in a number of Cr-doped media [31,32] as well as in Yb and Nd-doped media where it can be comparable or even stronger than the thermally-induced

Optics EXPRESS

lens [33,34]. The refractive index change is given by [33]

$$\Delta n_e(r,z) = \frac{2\pi}{n} f_L^2 N \Delta\alpha_p \frac{n_1(r,z)}{N} = C\frac{n_1(r,z)}{N} \tag{6}$$

where n is the unperturbed refractive index, $f_L = \left(n^2+2\right)/3$ is the Lorentz factor, N is the total active population density, $\Delta\alpha_p = \alpha_e - \alpha_g$ is the polarizability difference of the excited and ground state ions and $n_1(r,z)$ is the spatial profile of the excited state population density. The optical path wavefront due to the refractive index difference can be described by

$$W(r) = \int_0^l \Delta n_e(r,z)\,dz = C\int_0^l \frac{n_1(r,z)}{N}dz = CF(r) \tag{7}$$

where $F(r)$ is the integrated inversion factor over the gain medium of length l. Equation (7) can then be used to determine the optical path difference of the wavefront: $\Delta W = W(0) - W(r)$ which for a beam travelling through the gain medium acts as a lens of dioptric power

$$D_P = \frac{2}{r^2}\Delta W = \frac{2}{r^2}C\left(F(0) - F(r)\right). \tag{8}$$

Understanding the form of the population lens requires a detailed study of the population inversion which depends on a number of experimental conditions such as the pump intensity and absorption. Therefore it is of initial importance to consider the experimental setup and results before applying a specific theoretical framework. Detailed analysis of the integrated inversion factor F and treatment of a combined thermal and population lens under both non-lasing and lasing conditions will be provided later in Section 6.

3. Experimental systems and measurements

Figure 2(a) depicts the experimental setup used to measure the pump-induced lensing effects of an Alexandrite laser rod using the wavefront measuring approach with a Shack-Hartmann wavefront sensor (SH-WFS). The SH-WFS (Thorlabs, WFS20-7AR/M) measures the wavefront curvature enabling both the thermal lens dioptric power and aberrations to be determined. These are measured by passing a continuous-wave (CW) green probe beam (λ_{pr} = 532nm) through the crystal and imaging the pump region of the crystal onto the SH-WFS. The micro-lenslet array of the SH-WFS provides a 2-D set of local wavefront inclinations that can be interpolated to provide a reconstructed wavefront with sensitivity capability better than 100th of a wavelength.

The Alexandrite laser crystal was a plane-parallel rod with length 10 mm, radius 2 mm and nominal Cr-doping of 0.2 at.%. It was held in a water-cooled copper mount at 16 °C. The laser cavity consisted of a plane dichroic back mirror (BM) that was highly reflective (HR) at the laser wavelength ($\lambda_l \sim$ 755nm) and highly transmissive (HT) at the pump wavelength (λ_p = 635nm), and a plane mirror output coupler (OC) with a reflectivity of R_{OC} = 98.5% at the laser wavelength. The laser cavity length was L_C = 20 mm. The setup allowed the measurement of the thermal lens both with lasing and without lasing (by misaligning the OC).

The pump beam was from a CW fibre-delivered red diode laser operating at 635 nm. The fibre output was collimated and polarised with a polarising beam splitter such that the output was linearly polarised. A half-waveplate was used to rotate the polarisation to the high absorbing crystal b-axis. The absorption coefficient at the pump wavelength was measured to be α_0 = 480m^{-1}. The pump beam was focused near the input face of the laser rod with a 30 mm aspheric lens (f_1) to give a waist radius of w_p = 200µm. Figure 2(b) shows the pump beam intensity profile at focus. A best fit was performed with different Super-Gaussian functions $\exp(-2r^n/w_p^n)$ with the n = 2 order found to describe the intensity profile most accurately, as seen in the Gaussian (n = 2) fit to the data in Fig. 2(b). The pump beam quality was measured to be M^2 = 100.

Optics EXPRESS

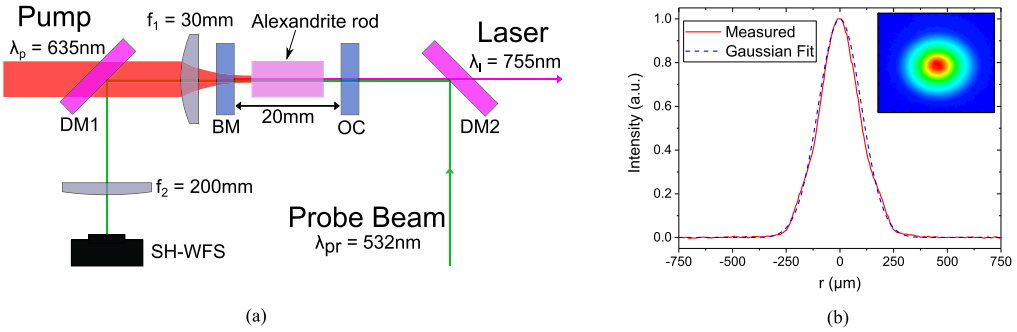

Fig. 2. (a) Schematic of the experimental pump-induced lensing measurement system of the end-pumped Alexandrite rod in a laser cavity (formed by mirrors BM and OC). f_1 and f_2 form an afocal magnifying telescope to relay-image a probe beam wavefront at the Alexandrite crystal onto a Shack-Hartmann wavefront sensor (SH-WFS). DM1 and DM2 are dichroic mirrors to separate pump, probe and laser wavelengths. (b) Measured radial intensity profile of the pump beam at focus (red line) together with a Gaussian ($n = 2$) fit (dashed blue line). Inset shows 2-D pump beam profile.

The probe beam was linearly polarised with its polarisation rotated to the crystal b-axis. The beam was collimated and its diameter adjusted to ~ 1 mm so that the beam overfilled the pump region. The probe beam at the pump face of the crystal was imaged using the combination of the 30 mm aspheric pump lens (f_1) and a 200 mm lens (f_2) onto the SH-WFS. A dichroic mirror (DM1) that was HR at the probe wavelength and HT at the pump wavelength was placed between the two lenses (as indicated in Fig. 2(a)) to separate the probe beam from the pump. An additional bandpass filter centred at 532 nm (FWHM=10 nm) was placed on the SH-WFS to further eliminate back scattered pump light and laser fluorescence/laser leakage.

The two lens arrangement served two purposes: (1) to relay image the wavefront aberration caused at the vicinity of the pump focal region onto the SH-WFS sensor plane; and (2) to provide a magnification factor $m = f_2/f_1$ of the lateral size of the pump beam region (diameter = 0.40 mm), to fill a suitable aperture size of the SH-WFS CMOS array. The $f_2 = 200$ mm lens was chosen in combination with the $f_1 = 30$ mm lens to provide a magnification of $m = 200/30 = 6.67$, therefore producing a magnified pump region of 0.40mm × 6.67 ~ 2.7 mm which fits comfortably inside the SH-WFS aperture (7.2 × 5.4 mm) and providing good lateral resolution across the discrete microlens array (SH-WFS pixel pitch 150 μm). The pupil size in the SH-WFS measurement software was fixed at 2.5 mm, corresponding to just within the magnified pump region in the experiment (~ 2.7 mm).

The relay image system with a magnification of m, produces an increase in the radius of curvature measured at the conjugate sensor plane of m^2. The measured SH-WFS wavefront measurements were rescaled by dividing with a scaling factor $m^2 = 44.5$ to obtain the focal length of the pump induced lens. As well as measuring the focal length, an assessment of the spherical aberration was also made. This is a key advantage of the SH-WFS compared to some simpler thermal lens measurement techniques.

The SH-WFS was initially calibrated by removing the laser rod and measuring the probe wavefront curvature after passing through five lenses of known focal lengths placed at the focal point of the pump lens coincident with the Alexandrite thermal lens region. The measured dioptric power was in excellent agreement with the actual lens dioptric power with the measurement coming to within 5 % of the actual value across the range of $D_{lens} = 0.5 - 20\text{m}^{-1}$ ($f_{lens} = 2000 - 50$ mm).

Optics EXPRESS

4. Results

4.1. Experimental results

The system shown in Fig. 2(a) was used to measure the dioptric lens power as a function of the absorbed pump power under non-lasing and lasing conditions. Figure 3 shows the dioptric power as a function of the absorbed pump power as well as the laser output power. It is clear that there is a very pronounced difference between the dioptric power under non-lasing and lasing conditions. To our knowledge, this is the first direct wavefront measurement of the thermal lens in Alexandrite and the first comparison of its thermal lensing under non-lasing and lasing conditions. We analyse the quality of the lensing, in particular its spherical aberration, in Section 7.

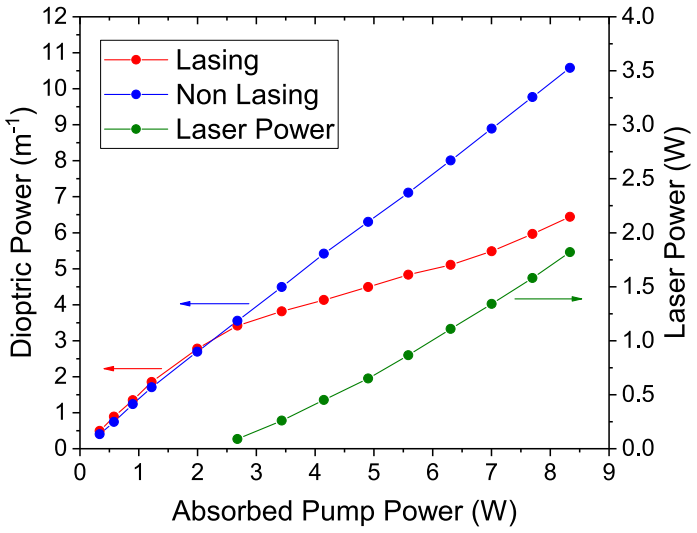

Fig. 3. Measured thermal lens dioptric power under non-lasing conditions (blue), lasing conditions (red) and laser power (green) as a function of the absorbed pump power.

The non-lasing lens dioptric power increases nearly linearly with absorbed pump power. Indeed it is slightly sub-linear (of the form $D_T = 1.34P_{abs} - 0.01P_{abs}^2$) in absorbed pump power. This pump dependence of the lensing dioptric power is not expected from the nonlinear pump ESA heating contribution discussed in Section 2.2. Under lasing conditions, the lens dioptric power however takes a very different behaviour diverging noticeably from the non-lasing case above laser threshold. At the maximum pump power (8.3 W) the dioptric power is 10.5 m^{-1} and 6.5 m^{-1} under non-lasing and lasing conditions, respectively. The lasing dioptric power is $\sim$ 60% of the non-lasing lens dioptric power.

Figure 4(a) shows the laser power as a function of the absorbed pump power. At a maximum pump power of 8.3 W the laser power was 1.82 W and an overall slope efficiency of $\eta_s = 30.8\%$ was determined from a linear fit. The beam quality was measured to be $M^2 = 1.1$ near threshold and at full pump power $M^2 = 1.5$. The laser spectrum (shown in inset of Fig. 4(a)) was centred at $\lambda_l = 755$nm with a linewidth of FWHM $\approx$ 3nm. Laser threshold was at an absorbed pump power of $P_{th} = 2.24$ W, this corresponds to the point where the lens dioptric power under lasing conditions deviates from that under non-lasing conditions (see Fig. 3). Figure 4(b) shows the 2-D wavefront acquired by the SH-WFS at maximum pump power with a noticeable stronger curvature measured under non-lasing conditions compared to that under lasing conditions.

Optics EXPRESS

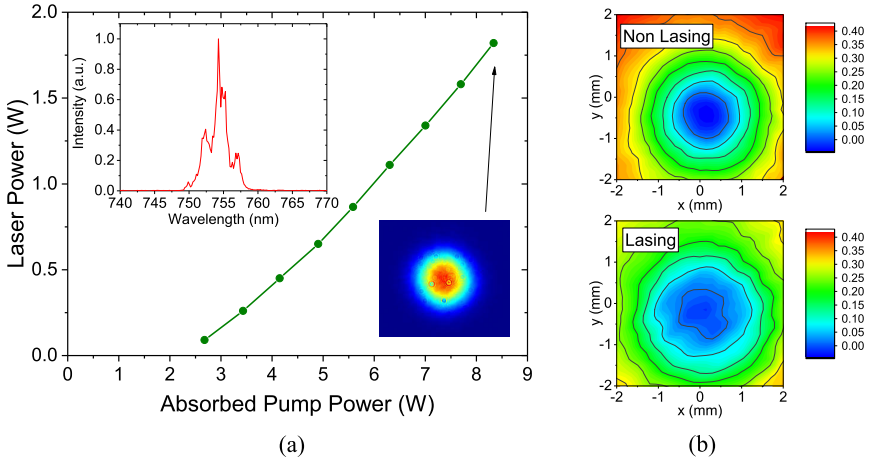

Fig. 4. (a) Laser power as a function of absorbed pump power. Inset shows laser wavelength spectrum and beam profile at maximum power. (b) 2-D wavefront at maximum pump power under non-lasing and lasing conditions.

4.2. FEA model

The low brightness (M^2 = 100) pump beam is not sufficiently well collimated in the gain medium to fully employ the analytical solutions of the thermal lens (Eq. (3)). A finite element analysis (FEA) numerical model was used to provide a more complete spatial model for the measured thermal lens dioptric power under non-lasing conditions. The FEA was performed using LASCAD software and used to compare to the experiment. Table 1 shows the parameters used for the FEA model with temperature dependent parameters evaluated at T = 16°C. This modelling was performed to deduce the fractional heating factor that brings agreement between the FEA model and experimental result, which we shall denote as the effective heating factor even though some of the physical origin of this factor may not be due to heat (as discussed later). The output of the FEA model provided a crystal 3-D refractive index profile. The parabolic fit of the FEA refractive index profile was chosen over the range r = 200µm to ensure a direct comparison with the pump waist (w_p = 200µm) that was measured in the magnified pupil size of the SH-WFS.

Figure 5 shows the effective heating factor as a function of the absorbed pump power under both non-lasing and lasing conditions that brings agreement between the experiment and the FEA model. The effective heating factor under non-lasing conditions is observed to be nearly constant at a value of ~ 33%. When lasing occurs the heating factor decreases with increasing pump power and then appears to plateau to ~ 20%, which is ~ 60% of the non-lasing value. The gradual decrease in the effective heating factor as opposed to a sudden decrease at the onset of lasing is due to two reasons. Firstly, at and near threshold there is a contribution due to fluorescence and this contribution does not abruptly decrease. Secondly, direct measurement of the laser mode size on the OC mirror suggests that the laser mode size was underfilling the pump mode size. Therefore, fluorescence will be present outside the pump and laser mode overlap. In the FEA model the surface bulge contribution to the lensing was found to be 10% of the total lens dioptric power and the remainder 90 % and dominant contribution was the temperature-dependent refractive index ($\chi_n = dn/dT$).

There are some uncertainties in the deduced heating factors due to limitations in the FEA model, which does not include a photoelastic contribution to the lensing and does not consider saturable absorption of the pump. The relevant photoelastic coefficients are not known for Alexandrite

Optics EXPRESS

Table 1. Alexandrite and pump parameters used for the FEA model. Temperature dependent parameters have been evaluated at T = 16 °C. Thermo-optic ceofficient (zero-strain) and refractive index is that for light polarised to the crystal b-axis at probe wavelength 532 nm.

Parameter	Symbol	Value	Source
Thermal conductivity	K_c	23 W m^{-1} K^{-1}	[13]
Thermo-optic coefficient (zero-strain)	dn/dT	9.1×10^{-6} K^{-1}	[25]
Young's modulus	E	4.69×10^{11} Pa	[13]
Refractive index	n	1.7518	[35]
Poisson's ratio	ν	0.25	Estimate
Coefficient of thermal expansion	α_T	6×10^{-6} K^{-1}	[13]
Fluorescence lifetime	τ_f	290 µs	[13]
Pump wavelength	λ_p	635 nm	-
Pump focal radius	w_p	200 µm	-
Pump beam quality	M^2	100	-
Absorption coefficient	α_0	480 m^{-1}	-

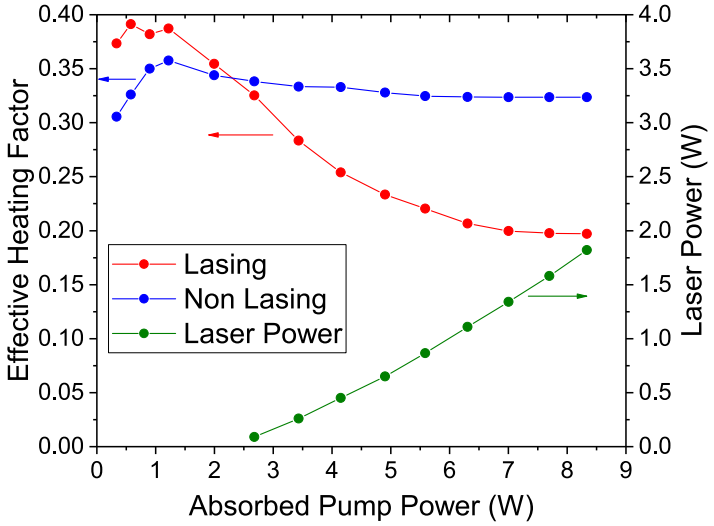

Fig. 5. Effective heating factor (fractional heating factor calculated from FEA model) under non-lasing (blue), lasing conditions (red) and laser power (green) as a function of the absorbed pump power.

but from data of other laser crystals, this contribution is likely to be in the range of 5 – 20% of the lensing [1]. Taking an additional 10 % photoelastic contribution to the thermal lens would reduce the effective heating factors to ~ 30% for the non-lasing case and ~ 18% for the lasing case. The FEA assumes simple exponential absorption of the pump which is only fully valid for pump intensities much less than the pump saturation intensity. In a simple four-level system, pump absorption saturation leads just to an effective increase in absorption depth. The presence of pump ESA reduces this extension of absorption depth. For $\gamma = \sigma_1/\sigma_0 = 1$, absorption depth becomes independent of inversion value. In Alexandrite, $\gamma \simeq 0.78$ [26] so simple exponential absorption is a reasonable assumption even under onset of pump saturation.

Optics EXPRESS

5. Heating factor with pump excited state absorption (ESA)

The fuller form of the heating factor was briefly discussed in Section 2.2. In this section we develop the mathematical formulation to deduce analytical expressions for the pump power dependence of the thermally-induced lens dioptric power. Under non-lasing conditions with pump ESA we can relate the pump ESA efficiency to the pump power using the following expressions from [30]

$$\eta_{p,esa} = \frac{1 - Te^{\sigma_1 NF}}{1 - T} \frac{\sigma_1 NF}{e^{\sigma_1 NF} - 1} \tag{9}$$

$$\frac{I}{I_s} = \frac{1}{1 - Te^{\sigma_1 NF}} \frac{e^{\sigma_1 NF} - 1}{\gamma} \tag{10}$$

where T is the pump transmission through the laser crystal, σ_1 is the pump ESA cross section, N is the total active ion population, $I_s = h\nu_p/\sigma_0\tau_f$ is the pump saturation intensity, $\gamma = \sigma_1/\sigma_0$ is the ratio of the pump ESA cross section to the pump GSA cross section and $F = \int_0^l f(z)\,dz$ is the integrated inversion factor. Simplification of Eqs. (9) and (10) can be made for a gain medium with strongly absorbed pump (T<<1) and not excessive pumping, i.e. $T\exp(\sigma_1 NF)$<<1. These conditions are well satisfied in the experiment with $T \approx \exp(-\alpha_0 l) = 0.8\%$ for $\alpha_0 = 480\text{m}^{-1}$ and $l = 0.01$m. Then from Eqs. (9) and (10)

$$\eta_{p,esa} \approx 1 - \frac{1}{2}\sigma_1 NF, \tag{11}$$

$$F \approx \frac{1}{\sigma_0 N}\left[\frac{I}{I_s} - \frac{\gamma}{2}\left(\frac{I}{I_s}\right)^2\right]. \tag{12}$$

Equations (11) and (12) can therefore be used to express the heating factor (using Eq. (4)) as a function of the incident pump intensity with the effect of pump ESA. To make analysis simpler we can limit ourselves to the on-axis case ($r = 0$). The heating factor in terms of the incident pump power P_0 and saturated power $P_s = I_s(\pi w_p^2/2)$ (see Appendix for derivation) is given by

$$\eta_h = 1 - \eta_s\eta_{p,esa} \approx 1 - \eta_s\left(1 - \frac{\gamma}{2}\left[\frac{P_0}{P_s} - \frac{\gamma}{2}\left(\frac{P_0}{P_s}\right)^2\right]\right) \tag{13}$$

Substituting Eq. (13) into Eq. (3) gives the on-axis thermal lens dioptric power including pump ESA heating and to second order in power (neglecting term proportional to P_0^3)

$$D_T(0) = \frac{\chi}{\pi w_p^2 K_c}\left[\eta_{h0}P_0 + \eta_s\frac{\gamma}{2}\frac{P_0^2}{P_s}\right] \tag{14}$$

where $\eta_{h0} = 1 - \eta_s$ and the Stokes efficiency is given by $\eta_s = \lambda_p/\lambda_f$ where λ_f is the average spontaneous emission wavelength ($\lambda_f = 732$nm in Alexandrite [13]). Equation (14) shows that under non-lasing conditions, pump ESA provides a quadratic power term and leads to a super-linear relationship between the thermal lens dioptric power and the absorbed pump power.

Figure 6 shows the fractional heating factor (Eq. (13)) as a function of the absorbed pump power for the Alexandrite setup in Section 3. A fuller numerical calculation using Eqs. (9) and (10) (dashed blue) is also shown for comparison. Initially the fractional heating factor is approximately equal to the quantum defect at $\eta_h \approx 1 - \eta_s = 0.13$ before gradually increasing to $\eta_h = 0.21$ at $P_{abs} = 8.3$W. The increasing heating factor and subsequent super-linear thermal lens dioptric power increase with absorbed pump power for Alexandrite is not consistent or able to describe the slightly sub-linear lens dioptric power measured in the experiment.

Optics EXPRESS

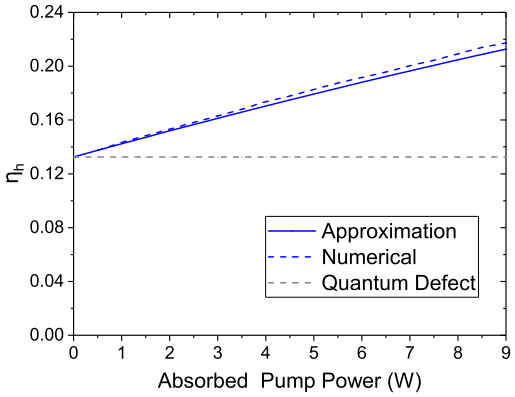

Fig. 6. Fractional heating factor as a function of absorbed pump power.

6. Thermal and population lens analytical model

6.1. Non-lasing conditions

To give a fuller description of the experimental pump-induced lens requires both a thermal and population lens to be considered. The analytical form of the population lens (Eq. (8)) introduced in Section 2.3 can be written in terms of the absorbed pump power using Eq. (12) for F (derivation shown in Appendix) and is given by

$$D_P(0) = \frac{4C}{\alpha_0 w_p^2}\left[\frac{P_0}{P_s} - \gamma\left(\frac{P_0}{P_s}\right)^2\right]. \tag{15}$$

It is noted that that the population lens dioptric power is sub-linear with pump power due to the negative sign in the quadratic power term P_0^2.

The total on-axis pump-induced lens under non-lasing conditions can be described by the sum of the thermal (Eq. (14)) and population lens (Eq. (15))

$$D_{\mathrm{NL}}(0) = \left[\frac{\chi\eta_{h_0}}{\pi w_p^2 K_c} + \frac{4C}{\alpha_0 w_p^2 P_s}\right]P_0 + \left[\frac{\chi}{\pi w_p^2 K_c}\frac{\gamma}{2}\frac{\eta_s}{P_s} - \gamma\frac{4C}{\alpha_0 w_p^2 P_s^2}\right]P_0^2. \tag{16}$$

From the near linearity of the non-lasing experimental lens dioptric power, it can be assumed that the quadratic coefficient in Eq. (16) is roughly zero. This provides an approximate expression for the population lens coefficient $C = \alpha_0\chi\eta_s P_s/8\pi K_c$ by equating the quadratic terms to zero. Substitution for C in the linear term gives

$$D_{\mathrm{NL}}(0) = \frac{\chi}{\pi w_p^2 K_c}\left[\eta_{h_0} + \frac{\eta_s}{2}\right]P_0 = \frac{P_0\chi\eta_h'}{\pi w_p^2 K_c} \tag{17}$$

where $\eta_h' = 0.57$ is the total apparent heating factor. In order to compare Eq. (17) to the measured result the divergence of the pump beam cannot be ignored. This can be incorporated by replacing the focused waist size w_p with an effective averaged waist size, w_p' given by [6,12]

$$w_p'^2 = \frac{\int_0^l \alpha_0 e^{\alpha_0 z} w^2(z)\,dz}{\int_0^l \alpha_0 e^{\alpha_0 z} dz} \tag{18}$$

which can be solved analytically to give $w_p' = 265\mu$m. The thermo-optic coefficient χ is calculated using $\chi_n = 9.1\times10^{-6}\mathrm{K}^{-1}$ (at probe wavelength 532 nm [25]), a 10 % contribution due the

Optics EXPRESS

surface bulging term χ_{SB} (from the FEA model) and an additional 10 % contribution due to the photo-elastic term χ_{PE} to give $\chi = 1.1 \times 10^{-5}\text{K}^{-1}$. Using this value deduces a population lens coefficient value $C = 1.4 \times 10^{-4}$ and hence $\Delta\alpha_p \sim 2.3 \times 10^{-31}\text{m}^3$. This result is consistent with the previously measured value of 2.7×10^{-31} m^3 [36] and the range of values measured for other Cr-doped material ($\sim 1 - 5 \times 10^{-31}\text{m}^3$) [31,37].

Figure 7 shows the measured thermal lens dioptric power (blue-solid) in comparison to the analytical formula using Eq. (16) (dashed-blue) as a function of the absorbed pump power. The population lens (green-dashed) and thermal lens (orange-dashed) components of the total lens dioptric power are also shown. The agreement between theory and experiment is excellent. The main fitting parameter was the population lens coefficient C, whose value gives a polarizability difference $\Delta\alpha_p$, as previously noted, consistent with prior literature for Cr-doped crystals.

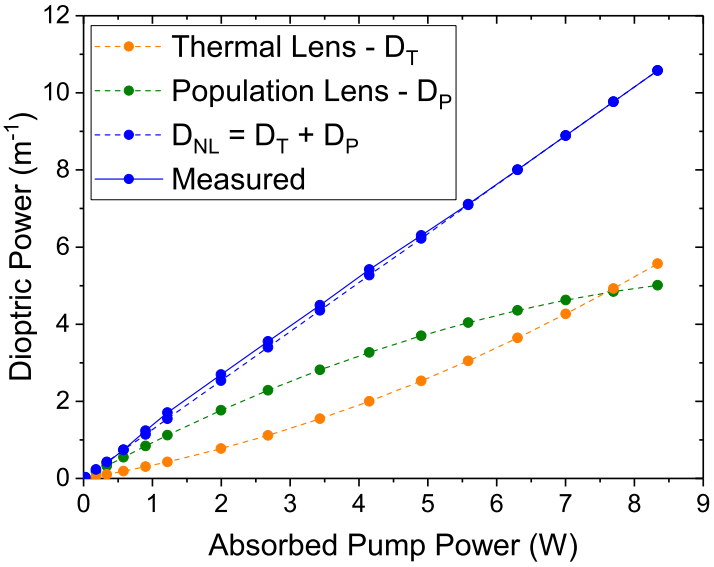

Fig. 7. Measured (blue-solid) and analytical (blue-dashed) lens dioptric power as a function of the absorbed pump power under non-lasing conditions. Thermal (orange-dashed) and population (green-dashed) lens components of the total lens are also shown.

6.2. *Lasing conditions*

To describe the pump-induced lens under lasing conditions the integrated inversion factor (Eq. (12)) is no longer dependent on the absorbed pump power and is instead clamped at threshold ($P_0 = P_{th}$) [26,30]. Although pump ESA is fixed at threshold, laser ESA and laser GSA provide an additional contribution to the heating factor. For Alexandrite under lasing conditions the heating factor varies between that at threshold given by Eq. (13) and a maximum value at far above threshold that is given by [26]

$$\eta_h = 1 - \eta_s \left(1 - \frac{\gamma}{2}\left[\frac{P_{th}}{P_s} - \frac{\gamma}{2}\frac{P_{th}^2}{P_s^2}\right]\right)(1 - \gamma_l) \tag{19}$$

where at far above threshold $\eta_s = \lambda_p/\lambda_l$ (λ_l is the laser wavelength) and $\gamma_l = \sigma_{1a}/(\sigma_e + \sigma_a)$ is the laser ESA fraction [26]. To describe the transition from non-lasing to strong lasing a power-dependent Stokes efficiency is defined as $\eta_s' = (1 - \eta_l)\lambda_p/\lambda_f + \eta_l\lambda_p/\lambda_l$ and the laser ESA fraction as $\gamma_l' = \eta_l\gamma_l$ where η_l is a lasing efficiency factor equal to the ratio of stimulated emission

Optics EXPRESS

to the total radiative emission (sum of spontaneous and stimulated emission). We take $\eta_l = 0$ up to $P_0 = P_{th}$ increasing linearly to $\eta_l = 1$ at the maximum pump power $P_0 = 8.3$W). In this experiment with the laser operating at $\lambda_l = 755$nm and at a temperature of $T = 16$°C, GSA is negligible, therefore $\gamma_l \approx \sigma_{1a}/\sigma_e \approx 0.12$ using $\sigma_{1a} = 0.57 \times 10^{-25}\text{m}^2$ and $\sigma_e = 4.95 \times 10^{-25}\text{m}^2$ from [38]. Using these parameters, substituting Eq. (19) into Eq. (3) gives the total pump-induced lens dioptric power under lasing conditions

$$D_L(0) = \frac{P_0 \chi}{\pi w_p^2 K_c}\left[\eta_{h0} + \eta_s' \frac{\gamma}{2}\frac{P_{th}}{P_s}\right](1-\gamma_l') + \frac{4C}{\alpha_0 w_p^2}\left[\frac{P_{th}}{P_s} - \gamma\frac{P_{th}^2}{P_s^2}\right] \tag{20}$$

where $\eta_{h0} = 1 - \eta_s'$. Equation (20) describes a lasing pump-induced lensing varying linearly with pump power P_0 and apparent heating term $\eta_h = (\eta_{h0} + \eta_s'\gamma P_{th}/2P_s)(1-\gamma_l')$ and an offset term that is proportional to the coupling constant C. Using the same parameters as under non-lasing conditions, Fig. 8 shows the total theoretical pump-induced lens (red-dashed) as a function of the absorbed pump power with thermal (orange-dashed) and population lens (green-dashed) components. The experimentally measured lens (red-solid) is also shown. The agreement is very good. In this case there was no re-adjustment of the fitting parameters, so it provides further independent support of the underlying hypothesis of a combined thermal and population lens.

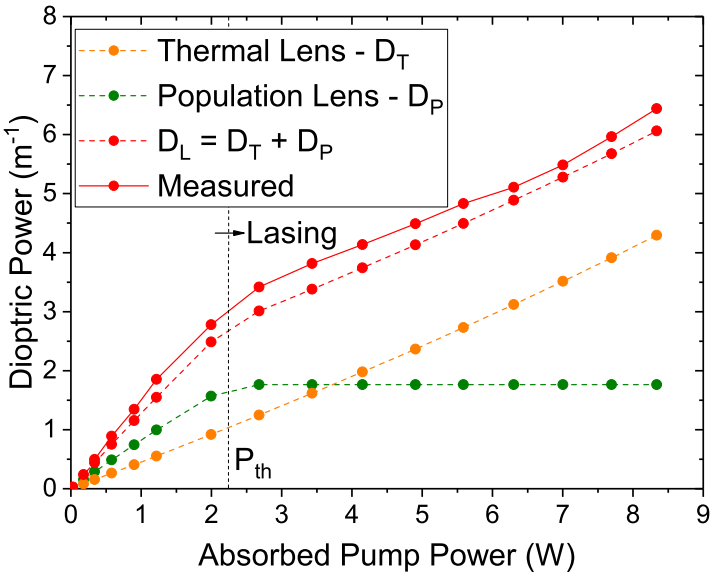

Fig. 8. Measured (red-solid) and analytical (red-dashed) lens dioptric power as a function of the absorbed pump power under lasing conditions. Thermal (orange-dashed) and population (green-dashed) lens components of the total lens are also shown.

7. Thermal aberrations

In addition to the thermal induced lens within the laser medium, spherical aberration is also one of the major obstacles for power scaling, particularly when the pump has a Gaussian profile. The phase distortion from a Gaussian intensity profile will give rise to high order aberrations, even in the case where the laser mode is less than the pump mode [2]. Direct measurement of the wavefront provides both validity of the thermal lens dioptric power measured and an indication of the strength of the aberrations with enables improved design in high power laser cavities. The SH-WFS software can be configured to represent the wavefront as a summation of Zernike

Optics EXPRESS

polynomials $W(r,\theta) = \sum_{n=0}^{\infty} c_n Z_n(r,\theta)$ where c_n is the nth Zernike coefficient and $Z_n(x,y)$ is the nth Zernike polynomial of order n. Minimising any misalignment tilts onto the wavefront sensor, the main Zernike coefficient is the $n = 5$th term, corresponding to defocus (lens dioptric power), and the $n = 13$th term, corresponding to spherical aberration. With only defocus and spherical aberration the wavefront aberration can be expressed as [2]

$$\Delta W = \frac{r^2}{2} D - w_{40} r^4 \tag{21}$$

where in the first term D is the defocus (lens dioptric power) and the second term represents spherical aberration, where w_{40} is the quartic aberration coefficient in the Seidal representation.

Figure 9 shows the wavefront measured by the SH-WFS (red) at maximum pump power (8.3 W), with Eq. (21) fitted to the measured data (blue). The quadratic defocus term (dashed green line) and spherical aberrations (dashed magenta line) quartic terms are also shown. The results shows good agreement between the theoretical fitting and the measured wavefront when only accounting for the defocus and spherical aberration. In both cases the wavefront has strong defocus around the pump region and a small amount of spherical aberration that increases significantly outside the pump region. The reduced defocus term in Fig. 9(b) compared to Fig. 9(a) again demonstrates the reduced pump-induced lensing under lasing conditions.

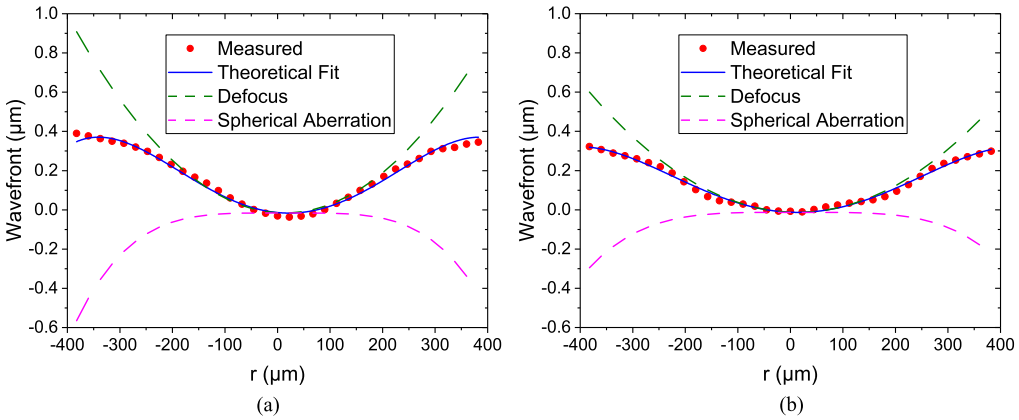

Fig. 9. Wavefront measured by the SH-WFS (shown in red) as a function of the radial coordinate, r, at the pump region at maximum pump power (8.3 W). A theoretical fitting applied to the data (shown in blue) is used to determine the lens dioptric power, D and quartic aberration coefficient, w_{40}, under non-lasing (a) and lasing conditions (b).

Performing the theoretical fitting shown in Fig. 9 across different pump powers allows the thermal lens dioptric power D and quartic aberration coefficient w_{40} to be determined as a function of the absorbed pump power as shown in Fig. 10(a). Up till and around laser threshold the aberration is similar under non-lasing and lasing conditions as expected. Above threshold the aberration under the two conditions deviate from one another with that under non-lasing conditions increasing at a larger rate due to the increased heating.

Figure 10(b) shows the thermal lens dioptric power determined from the theoretical fit (as in method used in Fig. 9) in comparison to the measured lens dioptric power as a function of the absorbed pump power under non-lasing and lasing conditions. Under both conditions the theoretical fitting gives a lens dioptric power that is slightly stronger than that in the experiment. This is to be expected as the theoretical fitting takes the axial (maximum) lens dioptric power rather than the measured experimental value which is averaged over the pump region.

Optics EXPRESS

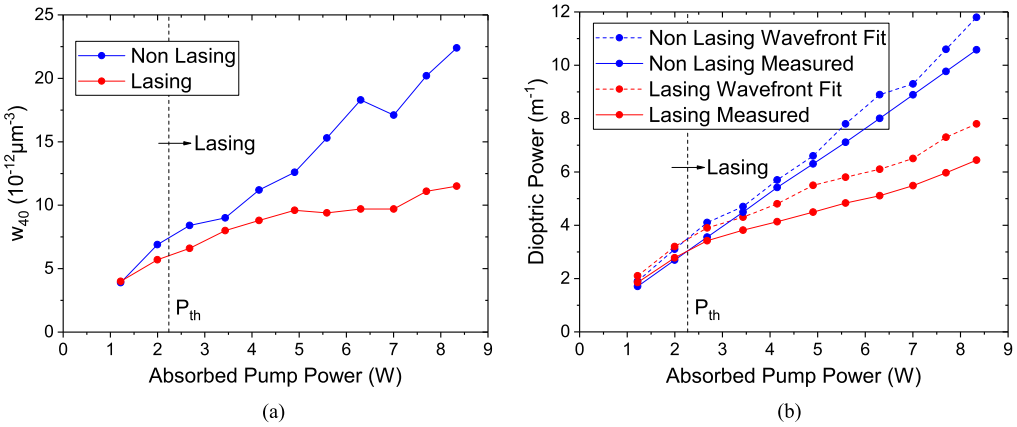

Fig. 10. (a) Quartic aberration coefficient as a function of absorbed pump power under non lasing and lasing conditions. (b) Measured (solid) and fitted thermal lens dioptric power (dashed) as a function of absorbed pump power.

8. Conclusion

This paper provides an in-depth investigation of pump-induced lensing effects in diode-end-pumped Alexandrite using a combined direct experimental measurement approach coupled to detailed analytical modelling and numerical finite element analysis (FEA). For the first time, we performed a direct wavefront measurement of pump-induced lensing in Alexandrite using a Shack-Hartmann wavefront sensor (SH-WFS). This provided both accurate lensing data from the direct high-sensitivity wavefront measurement afforded by the SH-WFS as well as information on lensing aberration, principally spherical aberration, that cannot be obtained easily by other less direct methods. Lensing measurements were performed as a function of absorbed pump power under both lasing and non-lasing conditions, again for the first time.

Some unexpected experimental results were obtained. The non-lasing lens dioptric power was found to grow slightly sub-linearly with pump power. This pump dependence is surprising as it is inconsistent with a theoretical prediction of nonlinear heating, due to pump excited state absorption (ESA) that is known to occur in Alexandrite, that should produce a super-linear lensing dependence with pump power. A further striking result found was that the lens dioptric power under lasing conditions was significantly different and reduced to 60 % of the value of the lens dioptric power under non-lasing conditions. The comparison of the lensing data to an FEA thermal modelling, that accounts for pump divergence and surface bulging effects, predicts there is an apparent heating factor $\sim$ 33% under non-lasing conditions. This apparent heating factor that brings the FEA modelling and experimental results into agreement is considerably higher than the non-lasing quantum defect which is $\sim$ 13%. These results together are hard to reconcile by a simple thermally-induced lens modelling, even if account is taken for some uncertainties in material values and experimental errors. It is however well-known that Cr-doped laser materials have previously been identified to possess an electronic component to their refractive index [31,37]. The origin of this effect is due to a difference in the polarizability of ions in the excited state to ions in the ground state. When pumping occurs, ground state population is transferred to the excited state and the local polarisation change leads to a refractive index change. For Cr-doped materials the refractive index is increased by population inversion and the refractive index distribution produced by a Gaussian pump beam leads to a positive "population" lens. In this paper, we performed a detailed pump-induced lensing analytical modelling of a thermal lens (with quantum defect and pump ESA heating) combined with a population lens. The modelling

Optics EXPRESS

makes use of analytical solutions for pump ESA quantum efficiency and its contribution to thermal heating factor [26,30]. Comparison of this modelling to experimental results provides for a good explanation for all the observed pump-induced measurements. The high apparent experimental heating factor ~ 33% deduced from comparison with FEA analysis is made up of a lower actual heating factor combined with a (non-thermal) population lensing factor. The near-linearity of the lens dioptric power with pump power (under non-lasing conditions) is accounted for by the combined thermal/population lensing. The thermal lens is super-linear with pump power due to the increasing inversion (and hence pump ESA heating contribution) but the population lens is sub-linear with pump power due to saturation of the inversion in the presence of strong pump ESA that occurs in Alexandrite. A good quantitative agreement can be obtained between the combined thermal/population lens model and experiment with a polarizability value for Alexandrite that is consistent with the range of values obtained by prior measurements for Cr-doped materials. The modelling was also modified to incorporate population clamping under lasing conditions. The model is found to provide good agreement with pump-induced lensing under lasing conditions. This agreement under lasing conditions provides further independent support for the hypothesis of the population lens.

The aberrations of the experimentally-measured pump-induced lensing is also analysed using a Seidal representation for the analysis of the radial shape of the wavefront. The pump-dependent wavefront is decomposed into a quadratic term (defocus) for the lens dioptric power and a quartic aberration coefficient that provides a measure of spherical aberration. Spherical aberration is seen to grow with pump power but also to reduce under lasing conditions.

The results of this study provide new insight into the pump-induced lensing in Alexandrite that should help to support future laser design for power scaling with high beam quality. However, a more significant factor of population lensing has been identified as a mechanism to provide explanation of the experimental non-lasing and lasing lensing results. A population lens is not unexpected for Cr-doped materials [37]. It would also provide a "fast" electronic modulation mechanism for self-Q-switching that has recently been observed to occur in Alexandrite lasers by ourselves and others [15,27], and where a population refractive index mechanism was postulated, but without experimental proof, as explanation. We would suggest that further corroborating experiment(s) should be made to directly observe the population lens, such as its temporal response compared to the build-up or decay of the thermal lens. The SH-WFS slow response time is not very suitable but with pulsed probe and/or pump or other experiments might be devised to make this temporal response measurement. Finally, the methodologies applied in this paper should be possible to extend to other laser materials.

Appendix

The fractional heating factor including a pump quantum efficiency for Alexandrite ($\eta_{p,0} = 1$) is given by $\eta_h = 1 - \eta_s\eta_p = 1 - \eta_s\eta_{p,esa}$. Substituting Eq. (11) for $\eta_{p,esa}$ gives

$$\eta_h = 1 - \eta_s\eta_{p,esa} \approx 1 - \eta_s\left(1 - \frac{1}{2}\sigma_1 NF\right) \tag{22}$$

Substituting for F using Eq. (12) gives

$$\eta_h = 1 - \eta_s\eta_{p,esa} \approx 1 - \eta_s\left(1 - \frac{\gamma}{2}\left[\frac{I}{I_s} - \frac{\gamma}{2}\left(\frac{I}{I_s}\right)^2\right]\right). \tag{23}$$

It is more convenient to write the fractional heating factor in terms of the pump power so that it can be compared to the experimental results. This can be done by setting $P_0 = I(\pi w_p^2/2)$ as the

Optics EXPRESS

absorbed pump power and $P_s = I_s(\pi w_p^2/2)$ as the pump saturation power. This gives

$$\eta_h = 1 - \eta_s\eta_{p,esa} \approx 1 - \eta_s\left(1 - \frac{\gamma}{2}\left[\frac{P_0}{P_s} - \frac{\gamma}{2}\left(\frac{P_0}{P_s}\right)^2\right]\right). \tag{24}$$

The population lens dioptric power is found by taking the radial form of Eq. (12)

$$F(r) \approx \frac{1}{\sigma_0 N}\left[\frac{I(r)}{I_s} - \frac{\gamma}{2}\left(\frac{I(r)}{I_s}\right)^2\right]. \tag{25}$$

Assuming a Gaussian pump profile $I(r) = (2P_0/\pi w_p^2)\exp(-2r^2/w_p^2)$ and with $P_s = I_s(\pi w_p^2/2)$

$$F(r) = \frac{\gamma}{\sigma_1 N}\left[\frac{P_0}{P_s}e^{-2r^2/w_p^2} - \frac{\gamma}{2}\left(\frac{P_0}{P_s}e^{-2r^2/w_p^2}\right)^2\right]. \tag{26}$$

Approximating $\exp(-2r^2/w_p^2) \approx 1 - 2r^2/w_p^2$ and $\exp(-4r^4/w_p^4) \approx 1 - 4r^2/w_p^2$ then

$$F(r) = \frac{1}{\sigma_0 N}\left[\left(\frac{P_0}{P_s} - \frac{\gamma}{2}\left(\frac{P_0}{P_s}\right)^2\right) - \frac{2r^2}{w_p^2}\left(\frac{P_0}{P_s}\gamma\left(\frac{P_0}{P_s}\right)^2\right)\right]. \tag{27}$$

Substituting Eq. (27) into Eq. (8) gives the on-axis population lens dioptric power

$$D_P(0) = \frac{4C}{\alpha_0 w_p^2}\left[\frac{P_0}{P_s} - \gamma\left(\frac{P_0^2}{P_s}\right)^2\right]. \tag{28}$$

Funding

Engineering and Physical Sciences Research Council (1858718); European Space Agency (4000115840/15/NL/PA/zk).

Disclosures

The authors declare no conflicts of interest.

References

1. W. Koechner, *Solid-state laser engineering* (Springer, 2006, 6 ed.).
2. W. A. Clarkson, "Thermal effects and their mitigation in end-pumped solid-state lasers," J. Phys. D: Appl. Phys. **34**(16), 2381–2395 (2001).
3. M. E. Innocenzi, H. T. Yura, C. L. Fincher, and R. A. Fields, "Thermal modeling of continuous-wave end-pumped solid-state lasers," Appl. Phys. Lett. **56**(19), 1831–1833 (1990).
4. B. Neuenschwander, R. Weber, and H. P. Weber, "Determination of the thermal lens in solid-state lasers with stable cavities," IEEE J. Quantum Electron. **31**(6), 1082–1087 (1995).
5. M. Schmid, T. Graf, and H. P. Weber, "Analytical model of the temperature distribution and the thermally induced birefringence in laser rods with cylindrically symmetric heating," J. Opt. Soc. Am. B **17**(8), 1398–1404 (2000).
6. S. Chenais, F. Balembois, F. Druon, G. Lucas-Leclin, and P. Georges, "Thermal lensing in diode-pumped ytterbium lasers-part i: theoretical analysis and wavefront measurements," IEEE J. Quantum Electron. **40**(9), 1217–1234 (2004).
7. S. Chenais, F. Druon, S. Forget, F. Balembois, and P. Georges, "On thermal effects in solid-state lasers: The case of ytterbium-doped materials," Prog. Quantum Electron. **30**(4), 89–153 (2006).
8. L. Cini and J. I. Mackenzie, "Analytical thermal model for end-pumped solid-state lasers," Appl. Phys. B: Lasers Opt. **123**(12), 273 (2017).
9. S. A. Amarande and M. J. Damzen, "Measurement of the thermal lens of grazing-incidence diode-pumped nd:yvo4 laser amplifier," Opt. Commun. **265**(1), 306–313 (2006).
10. D. C. Burnham, "Simple measurement of thermal lensing effects in laser rods," Appl. Opt. **9**(7), 1727–1728 (1970).

Optics EXPRESS

11. J. L. Blows, J. M. Dawes, and T. Omatsu, "Thermal lensing measurements in line-focus end-pumped neodymium yttrium aluminium garnet using holographic lateral shearing interferometry," J. Appl. Phys. **83**(6), 2901–2906 (1998).
12. S. Chenais, F. Balembois, F. Druon, G. Lucas-Leclin, and P. Georges, "Thermal lensing in diode-pumped ytterbium lasers-part ii: evaluation of quantum efficiencies and thermo-optic coefficients," IEEE J. Quantum Electron. **40**(9), 1235–1243 (2004).
13. J. Walling, O. Peterson, H. Jenssen, R. Morris, and E. O'Dell, "Tunable Alexandrite lasers," IEEE J. Quantum Electron. **16**(12), 1302–1315 (1980).
14. J. W. Kuper, T. Chin, and H. E. Aschoff, "Extended tuning range of alexandrite at elevated temperatures," in *Advanced Solid State Lasers*, (Optical Society of America, 1990, p. CL3.
15. I. Yorulmaz, E. Beyatli, A. Kurt, A. Sennaroglu, and U. Demirbas, "Efficient and low-threshold alexandrite laser pumped by a single-mode diode," Opt. Mater. Express **4**(4), 776–789 (2014).
16. A. Teppitaksak, A. Minassian, G. M. Thomas, and M. J. Damzen, "High efficiency >26w diode end-pumped alexandrite laser," Opt. Express **22**(13), 16386–16392 (2014).
17. W. R. Kerridge-Johns and M. J. Damzen, "Temperature effects on tunable cw alexandrite lasers under diode end-pumping," Opt. Express **26**(6), 7771–7785 (2018).
18. X. Sheng, G. Tawy, J. Sathian, A. Minassian, and M. J. Damzen, "Unidirectional single-frequency operation of a continuous-wave alexandrite ring laser with wavelength tunability," Opt. Express **26**(24), 31129–31136 (2018).
19. M. J. Damzen, G. M. Thomas, and A. Minassian, "Diode-side-pumped alexandrite slab lasers," Opt. Express **25**(10), 11622–11636 (2017).
20. G. M. Thomas, A. Minassian, X. Sheng, and M. J. Damzen, "Diode-pumped alexandrite lasers in q-switched and cavity-dumped q-switched operation," Opt. Express **24**(24), 27212–27224 (2016).
21. A. Munk, M. Strotkamp, M. Walochnik, B. Jungbluth, M. Traub, H.-D. Hoffmann, R. Poprawe, J. Höffner, and F.-J. Lübken, "Diode-pumped q-switched alexandrite laser in single longitudinal mode operation with watt-level output power," Opt. Lett. **43**(22), 5492–5495 (2018).
22. U. Parali, X. Sheng, A. Minassian, G. Tawy, J. Sathian, G. M. Thomas, and M. J. Damzen, "Diode-pumped alexandrite laser with passive sesam q-switching and wavelength tunability," Opt. Commun. **410**, 970–976 (2018).
23. S. Ghanbari, R. Akbari, and A. Major, "Femtosecond kerr-lens mode-locked alexandrite laser," Opt. Express **24**(13), 14836–14840 (2016).
24. C. Cihan, C. Kocabas, U. Demirbas, and A. Sennaroglu, "Graphene mode-locked femtosecond alexandrite laser," Opt. Lett. **43**(16), 3969–3972 (2018).
25. P. Loiko, S. Ghanbari, V. Matrosov, K. Yumashev, and A. Major, "Dispersion and anisotropy of thermo-optical properties of alexandrite laser crystal," Opt. Mater. Express **8**(10), 3000–3006 (2018).
26. W. R. Kerridge-Johns and M. J. Damzen, "Analytical model of tunable alexandrite lasing under diode end-pumping with experimental comparison," J. Opt. Soc. Am. B **33**(12), 2525–2534 (2016).
27. G. Tawy and M. J. Damzen, "Tunable, dual wavelength and self-q-switched alexandrite laser using crystal birefringence control," Opt. Express **27**(13), 17507–17520 (2019).
28. D. C. Brown, "Heat, fluorescence, and stimulated-emission power densities and fractions in nd:yag," IEEE J. Quantum Electron. **34**(3), 560–572 (1998).
29. S. Cante, S. J. Beecher, and J. I. Mackenzie, "Characterising energy transfer upconversion in nd-doped vanadates at elevated temperatures," Opt. Express **26**(6), 6478–6489 (2018).
30. W. R. Kerridge-Johns and M. J. Damzen, "Analysis of pump excited state absorption and its impact on laser efficiency," Laser Phys. Lett. **12**(12), 125002 (2015).
31. T. Godin, R. Moncorgé, J.-L. Doualan, M. Fromager, K. Ait-Ameur, R. A. Cruz, and T. Catunda, "Optically pump-induced athermal and nonresonant refractive index changes in the reference cr-doped laser materials: Cr:gsgg and ruby," J. Opt. Soc. Am. B **29**(5), 1055–1064 (2012).
32. E. Beyatli, A. Sennaroglu, and U. Demirbas, "Self-q-switched cr:licaf laser," J. Opt. Soc. Am. B **30**(4), 914–921 (2013).
33. O. L. Antipov, D. V. Bredikhin, O. N. Eremeykin, A. P. Savikin, E. V. Ivakin, and A. V. Sukhadolau, "Electronic mechanism for refractive-index changes in intensively pumped yb:yag laser crystals," Opt. Lett. **31**(6), 763–765 (2006).
34. E. Anashkina and O. Antipov, "Electronic (population) lensing versus thermal lensing in yb:yag and nd:yag laser rods and disks," J. Opt. Soc. Am. B **27**(3), 363–369 (2010).
35. P. Loiko and A. Major, "Dispersive properties of alexandrite and beryllium hexaaluminate crystals," Opt. Mater. Express **6**(7), 2177–2183 (2016).
36. V. Pilla, P. R. Impinnisi, and T. Catunda, "Measurement of saturation intensities in ion doped solids by transient nonlinear refraction," Appl. Phys. Lett. **70**(7), 817–819 (1997).
37. N. Passilly, E. Haouas, V. Ménard, R. Moncorgé, and K. Aït-Ameur, "Population lensing effect in cr:lisaf probed by z-scan technique," Opt. Commun. **260**(2), 703–707 (2006).
38. M. Shand and H. Jenssen, "Temperature dependence of the excited-state absorption of alexandrite," IEEE J. Quantum Electron. **19**(3), 480–484 (1983).